Journal of Magnetic Resonance **138,** 54–65 (1999)
Article ID jmre.1999.1710, available online at http://www.idealibrary.com on IDEAL®

Deuterium REDOR: Principles and Applications for Distance Measurements

I. Sack,* A. Goldbourt,† S. Vega,† and G. Buntkowsky*,[1]

*Institut für Organische Chemie der Freien Universität Berlin, Takustrasse 3, D-14195 Berlin, Germany; and †Weizmann Institute, Rehovot, Israel

Received July 27, 1998; revised December 15, 1998

The application of short composite pulse schemes (90°_x–90°_y–90°_x and 90°_x–180°_y–90°_x) to the rotational echo double-resonance (REDOR) spectroscopy of X–^{2}H (X: spin $\frac{1}{2}$, observed) systems with large deuterium quadrupolar interactions has been studied experimentally and theoretically and compared with simple 180° pulse schemes. The basic properties of the composite pulses on the deuterium nuclei have been elucidated, using average Hamiltonian theory, and exact simulations of the experiments have been achieved by stepwise integration of the equation of motion of the density matrix. REDOR experiments were performed on ^{15}N–^{2}H in doubly labeled acetanilide and on ^{13}C–^{2}H in singly ^{2}H-labeled acetanilide. The most efficient REDOR dephasing was observed when 90°_x–180°_y–90°_x composite pulses were used. It is found that the dephasing due to simple 180° deuterium pulses is about a factor of 2 less efficient than the dephasing due to the composite pulse sequences and thus the range of couplings observable by X–^{2}H REDOR is enlarged toward weaker couplings, i.e., larger distances. From these experiments the ^{2}H–^{15}N dipolar coupling between the amino deuteron and the amino nitrogen and the ^{2}H–^{13}C dipolar couplings between the amino deuteron and the α and β carbons have been elucidated and the corresponding distances have been determined. The distance data from REDOR are in good agreement with data from X-ray and neutron diffraction, showing the power of the method. © 1999 Academic Press

Key Words: **^{2}H REDOR; composite pulses; acetanilide; ^{13}C–^{2}H distances; ^{15}N–^{2}H distances.**

INTRODUCTION

In recent years solid state nuclear magnetic resonance (NMR) methods (*1–4*) have become an important tool for structure determination in solid systems, in particular when these systems exist in an amorphous or disordered phase, which cannot easily be studied by X-ray diffraction techniques. Moreover, solid state NMR has become, in conjunction with inelastic neutron scattering, the primary technique for studying proton or deuterium positions in solids, because of the well-known problem in locating hydrogen atoms of X-ray scattering. Some recent examples are the localization of protons or deuterons in H-bonded systems (*5, 6*).

There are two main interactions in NMR spectroscopy that can be used to determine X–^{1}H or X–^{2}H distances between an $I = \frac{1}{2}$ nucleus X and a neighboring proton or deuteron, namely, the chemical shift and the nuclear magnetic dipolar interaction. The value of the chemical shift interaction is very sensitive to structural features such as the primary and secondary structure of molecules. For example, it has been shown recently that isotropic ^{15}N chemical shielding can be used to determine ^{15}N–^{1}H or ^{15}N–^{2}H distances (*7, 8*). However, there is no easy direct way to interpret the CS data in terms of nuclear distances, because calibration measurements on systems with well-known distances are needed to correlate these data to distances. Nuclear dipolar interactions, on the other hand, give direct geometrical information about intra- or intermolecular distances. Thus the study of these interactions between ^{1}H–X and ^{2}H–X is generally much more informative than CS data.

For simple systems consisting of pairwise ^{2}H–X-labeled molecules, the values of dipolar interactions can be obtained by simply recording the static NMR powder spectra and analyzing their lineshapes (*9, 10*). It is advantageous to record the X-spin spectra, because it is nearly impossible to elucidate any dipolar couplings from broad ^{2}H spectra, because of the strong quadrupolar interactions of the deuterons. In many systems the dipolar interactions are much smaller than the chemical shift anisotropy of the X spin, making it difficult to resolve the dipolar interaction in static solid state NMR spectra. This problem was already overcome in the sixties by the introduction of the spin echo double-resonance experiment (SEDOR) (*11*) technique and by separated local field experiments (*12, 13*).

When more complicated systems with several inequivalent deuterons and/or X nuclei are investigated, or when it is not possible to label only the interesting ^{2}H positions, special high-resolution solid state NMR techniques can be employed. By far the most important of these techniques is the rotational echo double-resonance (REDOR) experiment (*14, 15*), which monitors the dipolar interaction of spin pairs during magic angle spinning (MAS), often combined with proton–X cross-polarization (CP-MAS) (*16*) to enhance the X-spin signals. The dipolar REDOR dephasing of the signals is accomplished by the application of two 180° inversion pulses during each rotor period.

[1] To whom correspondence should be addressed.

1090-7807/99 $30.00

So far, most REDOR studies have been concerned with *IS* pairs of spin-$\frac{1}{2}$ nuclei, the main reason being that the large quadrupolar interaction of spins with $S > \frac{1}{2}$ complicates the interpretation of the REDOR data, because of the inefficient inversion of the 180° pulses on these nuclei. For spin pairs with $S > 1$ it is now common to apply the rotational echo adiabatic pulse double-resonance (REAPDOR) method (*17*, *18*).

For the study of the spin pair X–^{2}H (with $S = \frac{1}{2}$ and $I = 1$), two REDOR schemes have been suggested: the observation of the ^{2}H nucleus, while all 180° pulses are applied to the X nucleus (*19*), or the observation of the X nucleus, while the ^{2}H nucleus is pulsed (*19–23*). The advantage of the first experiment is that only moderate B_1 fields that are larger than the CSA dispersion are sufficient for spin inversion. In this REDOR experiment the presence of ^{2}H quadrupolar interaction of order 100–200 kHz results in ^{2}H MAS spectra with ca. 20–40 rotational sidebands for moderate spinning frequencies of ~5 kHz. The widths of these sidebands make it difficult to resolve the spectra of different ^{2}H sites in the sample. Spectral resolution between different ^{2}H sites therefore requires selective deuterium labeling. However, this is feasible only in some fortunate cases, while for the majority of systems it is scarcely achieved. For example, most of the hydrogens involved in the formation of H bridges are easily exchanged and selective labeling of X–^{2}H spin pairs is impossible or at least a severe synthetic problem.

From these considerations it follows that REDOR experiments that monitor the X nuclei and irradiate the ^{2}H nuclei hold promise for X–^{2}H REDOR spectroscopy (*19–23*). In experiments of these types, it is possible to measure the dipolar couplings even when several inequivalent deuterons are present. However, the problem with this approach is that very strong B_1 fields are necessary for faithfully inverting the ^{2}H nuclei, something that is not available in commercial triple-tuned probes.

The application of phase cycling schemes (*24*), such as *XY*-8 or *XY*-16, is not sufficient to compensate for the influence of the large quadrupolar broadening on the REDOR decays. These schemes are used mainly to correct pulse imperfections and the effects of small CS values. A solution to this problem is to use composite inversion pulses (*25–27*). To improve the X-spin REDOR dephasing, composite pulses can be used to substitute the simple 180° pulses on the deuterium spins. For nonrotating samples there are several elaborate composite pulse schemes available for the inversion of quadrupolar spin-1 nuclei (*26*, *27*). For rotating samples only the short composite sequences are suitable, due to the time restrictions implied by the sample rotation.

We have explored this experimentally by performing studies of ^{15}N–^{2}H in doubly labeled and ^{13}C–^{2}H in singly and doubly labeled acetanilide. To analyze the REDOR decay signals we have simulated the evolution of these data, using a numerical integration of the equation of motion of the density matrix. In addition, average Hamiltonian theory is used to understand the main features of the X-spin REDOR decays.

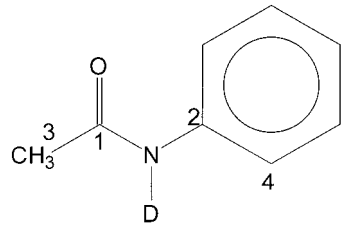

FIG. 1. Molecular structure of acetanilide.

Acetanilide (Fig. 1) has been chosen for several reasons: (i) it has only one exchangeable hydrogen, which makes specific labeling easy; (ii) it is a molecule with a large deuterium quadrupolar interaction (146 kHz) and with different types of carbons, making it a good example for this type of experiment; (iii) it has a known crystal structure (*28–30*), allowing a comparison of NMR and diffraction results; and (iv) it has favorable NMR parameters, such as relatively short relaxation times and well-separated ^{13}C spectral lines (*9*, *10*).

The rest of the article is organized as follows. After this Introduction, the theoretical background necessary for understanding REDOR measurements on X–^{2}H spin systems is given, followed by the numerical methods used. After an overview of the experimental setup, experimental results are presented, discussed, and summarized.

THEORY

Pulse Sequences

As mentioned before, the main problem of X-spin-detected X–^{2}H REDOR experiments is the relatively low B_1 field strength that can be obtained in our triple-tuned probes for the excitation of the deuterons. In our case the ^{2}H B_1 field was between 30 and 40 kHz, which is about four to five times smaller than the ^{2}H quadrupolar interaction in our samples. This leads to poor excitation of the ^{2}H NMR spectrum. This situation is a little improved in MAS experiments, where the quadrupolar frequencies are time-dependent during the pulses; however, in rotor-synchronized irradiation schemes the spins are always excited when they experience the same frequencies. To improve this excitation profile we performed experiments and calculations with composite pulse sequences. In the literature one can find a variety of composite pulse sequences that are efficient for the inversion of ^{2}H nuclei in nonrotating samples (*26*, *27*). The application of these sequences in MAS experiments is generally not feasible when the length of the sequence becomes comparable to the rotation period. We therefore chose to use the simple composite sequences 90_x–180_y–90_x and 90_x–90_y–90_x for the inversion of the ^{2}H nuclei. The actual pulse schemes used for the irradiation in our REDOR experiments are shown in Fig. 2.

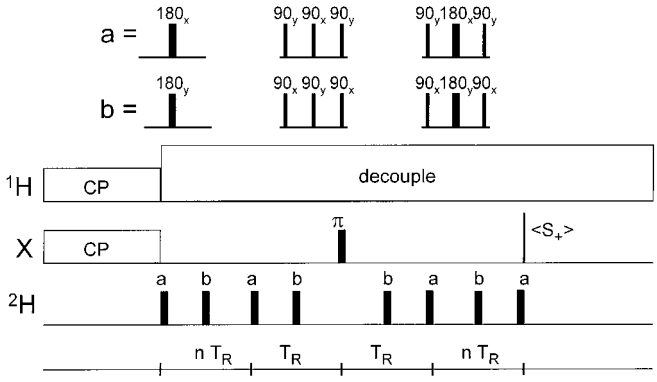

FIG. 2. Pulse sequences used for the X–^{2}H REDOR experiments.

A heteronuclear spin pair with a spin-$\frac{1}{2}$ nucleus I (for example, ^{13}C or ^{15}N) coupled to a spin-1 nucleus S (for example, ^{2}H) in a solid has a high-field MAS NMR Hamiltonian of the form

$$H(t) = \omega_D(t) \cdot 2I_zS_z + \tfrac{1}{3}\omega_Q(t)(3S_z^2 - 2) + H_{RF}(t), \quad [1]$$

where the last term represents a set of RF pulses applied to both spins and the time-dependent coefficients are due to the sample spinning; $\omega_Q(t)$ is the quadrupolar interaction and $\omega_D(t)$ the dipolar coupling between the I and S spins. Terms corresponding to off-resonance and chemical shift anisotropy parameters are not essential for the forthcoming discussion and are therefore omitted.

The dipolar coupling coefficient $\omega_D(t)$ depends on the distance between the two spins and the time-dependent angle $\vartheta(t)$ between the internuclear vector and the external magnetic field:

$$\omega_D(t) = \frac{\mu_0}{4}\hbar\frac{\gamma^I\gamma^S}{r^3}(3\cos(\vartheta(t))^2 - 1)$$
$$= \frac{D}{2}(3\cos(\vartheta(t))^2 - 1). \quad [2]$$

Detection of the D coefficient provides the internuclear distance. The sample spinning removes the effect of D on the MAS FID signal by averaging the dipolar interaction to zero. The effect can be recovered by applying a set of RF pulses that interferes with the averaging of the dipolar interaction in the course of the MAS experiment and results in an effective dipolar signal decay.

Numerical Methods

For full quantitative evaluation of the X–^{2}H REDOR data, numerical simulations are necessary. These are done by solving the equation of motion of the density matrix of the two-spin system considering all experimental parameters, such as the sample rotation frequency, the RF irradiation pulse lengths and intensities, and the quadrupolar interaction strength. For a variety of dipolar interactions REDOR decay curves were calculated and compared with the experimental results. Because of the quadrupolar interaction and the relatively low RF fields, the universal REDOR $\Delta S/S$ curve (*14*, *15*) cannot be used in this case.

The spin propagators for one rotation period of the different steps of the experiment have been calculated by stepwise numerical integration ($\Delta\tau = 1$ μs constant time steps) of the spin density matrix equation. The REDOR decay signals were evaluated as a function of the number of rotor cycles by repeated application of these propagators. The B_1 field strength in the calculations was chosen in such a way that the products of the experimental duration of the RF pulses and the B_1 field are equal to π or $\pi/2$ (i.e., $\gamma B_1\, n\Delta\tau = \pi$ or $\pi/2$) for spins on resonance. For the powder integration, summations of the signals from single crystallites, defined by their Euler angles in the rotor frame, were performed using the method of Cheng *et al.* (*31*). The set with 200 triples of Euler angles was used to simulate the data in the course of the data-fitting process. This was sufficient to give a good approximation of the experimental data in a reasonable CPU time. The final simulations were performed with the set of 1154 angle triples. The typical time for a simulation of a decay curve is approximately 750 s on a Pentium 200. The errors of the determined dipolar couplings have been estimated by determining upper and lower limits of the dipolar coupling strengths such that 70% of the experimental data are enclosed within the limiting curves.

The Average Hamiltonian

Further insight into the effect of the application of composite pulses to the S-spin system can be gained by analyzing the average Hamiltonians of the spin system. To evaluate the response of the spin system to the Hamiltonian in Eq. [1] it is most convenient to eliminate the RF term by transforming it to the toggling frame (*32*). This can easily be accomplished by transforming the linear and bilinear operators in Eq. [1] according to the applied pulse sequence with

$$I_z(t) = \sum_{p=x,y,z} f_p(t)I_p, \quad S_z(t) = \sum_{p=x,y,z} g_p(t)S_p, \quad [3]$$

resulting in the toggling frame Hamiltonian (*33*, *34*)

$$H^T = \sum_{p,q=x,y,z} \omega_D(t)\, f_p(t)\, g_q(t)$$
$$\times 2I_pI_q + \tfrac{1}{3}\sum_{p,q=x,y,z} \omega_Q(t)(3g_{pq}(t)S_pS_q - 2), \quad [4]$$

with $g_{pq}(t) = g_p(t)g_q(t)$.

For XY-4 REDOR experiments, with ideal 180° pulses applied only to the S spin, the $g_z(t)$ coefficient becomes a simple step function equal to ± 1, changing sign at the posi-

tions of the pulses (*33, 34*). All other coefficients are zero, except $f_z(t) = 1$ and $g_{zz}(t) = 1$, and therefore the Hamiltonian for this case becomes

$$H^{\mathrm{T}}(t) = \omega_{\mathrm{D}}(t)\, g_z(t) \cdot 2I_zS_z + \tfrac{1}{3}\omega_{\mathrm{Q}}(t)(3S_z^2 - 2). \qquad [5]$$

This Hamiltonian commutes with itself at all times and its average Hamiltonian for one rotor cycle becomes (*32*)

$$H^{(0)} = \tilde{\omega}_{\mathrm{D}} I_z S_z \quad \text{with}$$
$$\tilde{\omega}_{\mathrm{D}} = \frac{2}{T_2}\left(-\int_0^{T_{\mathrm{R}}/2} \omega_{\mathrm{D}}(t)dt + \int_{T_{\mathrm{R}}/2}^{T_{\mathrm{R}}} \omega_{\mathrm{D}}(t)dt \right), \qquad [6]$$

where $\tilde{\omega}_{\mathrm{D}}$ is the orientation-dependent REDOR frequency for a single crystallite.

To proceed it is useful to rewrite the Hamiltonian in terms of fictitious spin-half operators. Assuming a numbering of the eigenstates as

$$1 \equiv |\alpha, 1\rangle;\ 2 \equiv |\alpha, 0\rangle;\ 3 \equiv |\alpha, -1\rangle;$$
$$4 \equiv |\beta, 1\rangle;\ 5 \equiv |\beta, 0\rangle;\ 6 \equiv |\beta, -1\rangle, \qquad [7]$$

the Hamiltonian in Eq. [1] can be expressed in the convenient form (omitting the RF term)

$$H(t) = H^{\alpha}(t) + H^{\beta}(t)$$
$$H^{\alpha}(t) = 2\omega_{\mathrm{D}}(t) I_z^{13} + \tfrac{2}{3}\omega_{\mathrm{Q}}(t)(I_z^{12} - I_z^{23})$$
$$H^{\beta}(t) = -2\omega_{\mathrm{D}}(t) I_z^{46} + \tfrac{2}{3}\omega_{\mathrm{Q}}(t)(I_z^{45} - I_z^{56}) \qquad [8]$$

and can be represented in matrix form as

$$H(t) = \begin{bmatrix} H^{\alpha}(t) & 0 \\ 0 & H^{\beta}(t) \end{bmatrix}, \qquad [9]$$

where the $H^{\alpha}(t)$ and $H^{\beta}(t)$ operators are 3×3 matrices in the S-spin basis states with $m_I = \frac{1}{2}$ and $m_I = -\frac{1}{2}$, respectively. The linear I_x operator can be expanded as

$$I_x = I_x^{14} + I_x^{25} + I_x^{36} \qquad [10]$$

and is proportional to the initial density matrix ρ_0 after the CP-MAS excitation of the I spin. In this representation the three terms of I_x connect states corresponding to m_S equal to 1, 0, and -1, respectively.

The zero-order Hamiltonian in Eq. [6] can be rewritten as

$$H^{(0)} = \tilde{\omega}_{\mathrm{D}}(I_z^{13} - I_z^{46}) = \tilde{\omega}_{\mathrm{D}}(I_z^{14} - I_z^{36}), \qquad [11]$$

influencing only the I_x^{14} and I_x^{36} parts of the initial density matrix. This shows that the I-spin-detected REDOR signal decays only to $\frac{1}{3}$,

$$S^{\mathrm{REDOR}}(nT_{\mathrm{R}}) = \tfrac{1}{3} + \tfrac{2}{3}\cos(n\tilde{\omega}_{\mathrm{D}}T_{\mathrm{R}}), \qquad [12]$$

leaving the I_x^{25} term of the density matrix untouched.

In the case of pulses with finite lengths the form of the toggling frame Hamiltonian becomes more complicated, and the coefficients $f_p(t)$ and $g_p(t)$ have to be calculated explicitly. In this publication we will discuss two examples of I-spin-detected REDOR experiments on an I–S spin system with all pulses on the $S = 1$ spin, implying that $f_{x,y}(t) \equiv 0$ and $f_z(t) \equiv 1$. In particular we will discuss the effect of the average toggling frame Hamiltonian on the REDOR decay of the X-spin signal.

XY-4 REDOR

First we consider the REDOR experiment with four XY-4 180° pulses applied to the S spin during two rotor cycles. In Fig. 3 the time-dependent $g_p(t)$ and $g_{pq}(t)$ coefficients (see also Appendix A for the explicit form of the $g_p(t)$ and $g_{pq}(t)$) for the toggling frame Hamiltonian of Eq. [4] are shown.

A zero-order average Hamiltonian can then be obtained by integration of its coefficients over the two rotor periods. The resulting coefficients are functions of the exact forms of the dipolar and quadrupolar coefficients. Simple inspection shows that the terms involving $g_x(t)$, $g_y(t)$, $g_{xz}(t)$, $g_{yz}(t)$, and $g_{xy}(t)$ do not contribute to $H^{(0)}$. The remaining terms result in an average Hamiltonian of the form

$$H^{(0)} = H^{\alpha(0)} + H^{\beta(0)}$$
$$H^{\alpha(0)} = \tilde{\omega}_{\mathrm{D}} I_z^{13} + \tilde{\omega}_{zz}(I_z^{12} - I_z^{23}) + \tilde{\omega}_{xx} I_x^{13}$$
$$H^{\beta(0)} = -\tilde{\omega}_{\mathrm{D}} I_z^{46} + \tilde{\omega}_{zz}(I_z^{45} - I_z^{56}) + \tilde{\omega}_{xx} I_x^{46} \qquad [13]$$

with

$$I_x^{13} + I_x^{46} = \tfrac{1}{2}(S_x^2 - S_y^2)$$
$$(I_z^{12} - I_z^{23}) + (I_z^{45} - I_z^{56}) = 3S_z^2 - 2 \qquad [14]$$

and

$$\tilde{\omega}_{\mathrm{D}} = \frac{1}{T_{\mathrm{R}}}\int_0^{2T_{\mathrm{R}}} g_z(t)\,\omega_{\mathrm{D}}(t)dt$$

$$\tilde{\omega}_{zz} = \frac{1}{3T_{\mathrm{R}}}\int_0^{2T_{\mathrm{R}}} \left\{ g_{zz}(t) - \frac{1}{2}(g_{xx}(t) + g_{yy}(t)) \right\} \omega_{\mathrm{Q}}(t)dt$$

$$\tilde{\omega}_{xx} = \frac{1}{2T_{\mathrm{R}}}\int_0^{2T_{\mathrm{R}}} (g_{xx}(t) + g_{yy}(t))\,\omega_{\mathrm{Q}}(t)dt. \qquad [15]$$

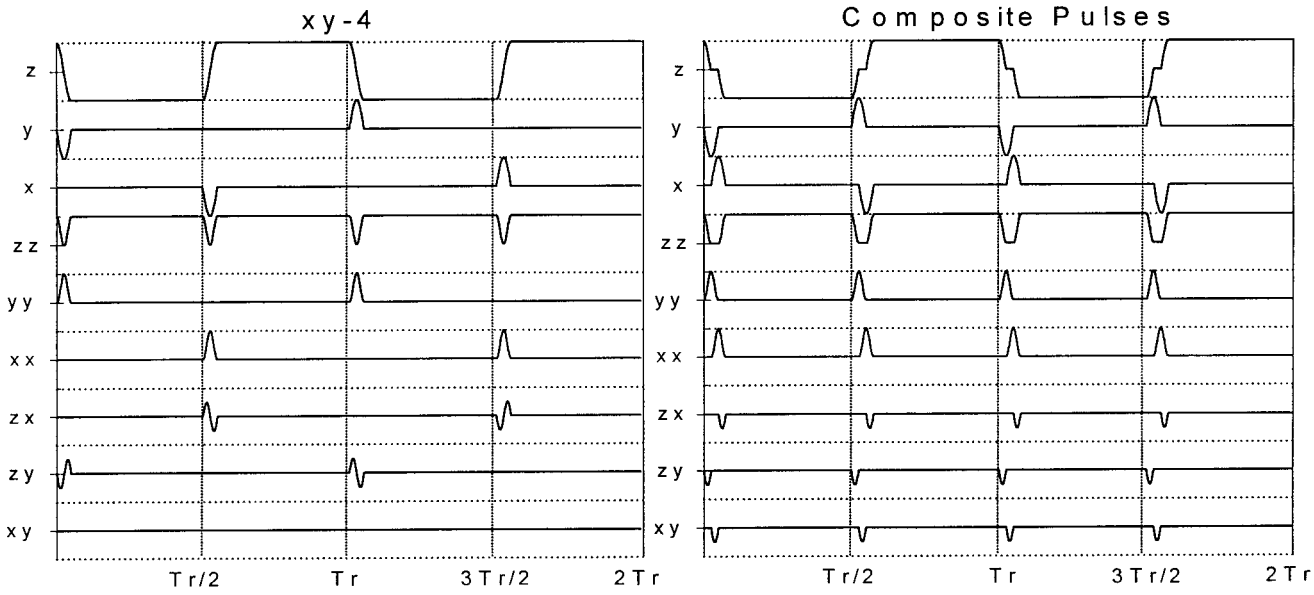

FIG. 3. Time-dependent $g_p(t)$ and $g_{pq}(t)$ coefficients ($p, q = x, y, z$) of the toggling frame Hamiltonian, Eq. [4]. Left, *XY*-4 REDOR; right, CPL REDOR. An explicit description of the time dependence of the coefficients is given in Appendix A.

The finite pulse lengths influence the average Hamiltonian in Eq. [6] by reducing the dipolar frequency $\tilde{\omega}_D$ and by adding a quadrupolar and a double-quantum term. While the $\tilde{\omega}_{zz}$ term has no effect on the *I*-spin signal, the $\tilde{\omega}_{xx}$ double-quantum term can have a large effect. For the extreme case $\omega_Q \gg \omega_1$ it follows that $\tilde{\omega}_D \ll \tilde{\omega}_{xx}$ and the double-quantum elements $\tilde{\omega}_{xx} I_z^{13,46}$ become the dominant term in $H^{(0)}$. In that case $H^{\alpha(0)} \cong H^{\beta(0)}$ and the initial spin density matrix is hardly influenced by $H^{(0)}$. The exact zero-order solution for the problem is calculated by diagonalizing the Hamiltonian. A straightforward calculation reveals that the REDOR signal of a single crystallite develops as (again $S(0) = 1$)

$$S^{\mathrm{REDOR}}(2nT_R) = \frac{1}{3} + \frac{2}{3}\left(\cos^2\phi \cos(\tilde{\omega}_D^{\mathrm{eff}} \cdot 2nT_R) + \sin^2\phi\right)$$

$$\tan^{-1}\phi = \frac{\tilde{\omega}_{xx}}{\tilde{\omega}_D}; \quad \omega_D^{\mathrm{eff}} = \sqrt{\tilde{\omega}_D^2 + \tilde{\omega}_{xx}^2}. \qquad [16]$$

The I_x^{25} term of the density matrix remains unaffected and the powder signal reaches a value of $\frac{1}{3} + \frac{2}{3}\langle \sin^2\phi \rangle$, where $\langle \sin^2 \phi \rangle$ is the powder average of the sine squares for all single crystallites. In a powder sample the different crystallites will decay with different rates and will reach different values, depending on their $\omega_Q(t)$ values. The overall decay of the REDOR powder signal for large quadrupolar interactions will therefore slow down and will not reach the $\frac{1}{3}$ value, as expected for small quadrupolar interactions.

Composite Pulse REDOR

The use of composite pulses will increase the inversion efficiency of the 180° pulses on *S* spins with large quadrupolar frequencies and will generate *I*-spin REDOR signals that approach the zero-quadrupolar REDOR decay curves. As expected these pulses result in an increase of the overall rate of the powder REDOR decay. In addition they cause the REDOR signals to decrease beyond $\frac{1}{3}$, indicating a decay of the I_x^{25} terms of the density matrix. In order for the I_x^{25} part of the *I* spins to decay, additional terms must appear in the average Hamiltonian. A term of the form I_z^{25} in $H^{(0)}$ could cause this additional decay; however, this operator does not appear in the zero-order Hamiltonian, because the quadrupolar terms in the H^α and H^β blocks must have the same form. We therefore expect that other types of interaction terms influence the I_x^{25} coherence. To demonstrate this we choose to describe the composite pulse REDOR sequence,

$$\{90_y 90_x 90_y\} - \tfrac{1}{2}T_R - \{90_x 90_y 90_x\} - \tfrac{1}{2}T_R - \{90_y 90_x 90_y\} - \tfrac{1}{2}T_R - \{90_x 90_y 90_x\} - \tfrac{1}{2}T_R, \qquad [17]$$

and show in Fig. 3 the $g_p(t)$ and $g_{pq}(t)$ coefficients of its $H^T(t)$ (see also Appendix A for the explicit form of $g_p(t)$ and $g_{pq}(t)$). The toggling frame Hamiltonian in this case has the same form as in Eq. [4], and the zero-order average Hamiltonian becomes

$$\begin{aligned} H^{(0)} &= H^{\alpha(0)} + H^{\beta(0)} \\ H^{\alpha(0)} &= \omega_D^{(0)} I_z^{13} + \omega_{zz}^{(0)}(I_z^{12} - I_z^{23}) + \omega_{xx}^{(0)} I_x^{13} \\ &\quad + \omega_{xy}^{(0)} I_y^{13} + \omega_{xz}^{(0)}(I_x^{12} - I_x^{23}) + \omega_{yz}^{(0)}(I_y^{12} - I_y^{23}) \\ H^{\beta(0)} &= -\omega_D^{(0)} I_z^{46} + \omega_{zz}^{(0)}(I_z^{45} - I_z^{56}) + \omega_{xx}^{(0)} I_x^{46} \\ &\quad + \omega_{xy}^{(0)} I_y^{46} + \omega_{xz}^{(0)}(I_x^{45} - I_x^{56}) + \omega_{yz}^{(0)}(I_y^{45} - I_y^{56}) \end{aligned} \qquad [18]$$

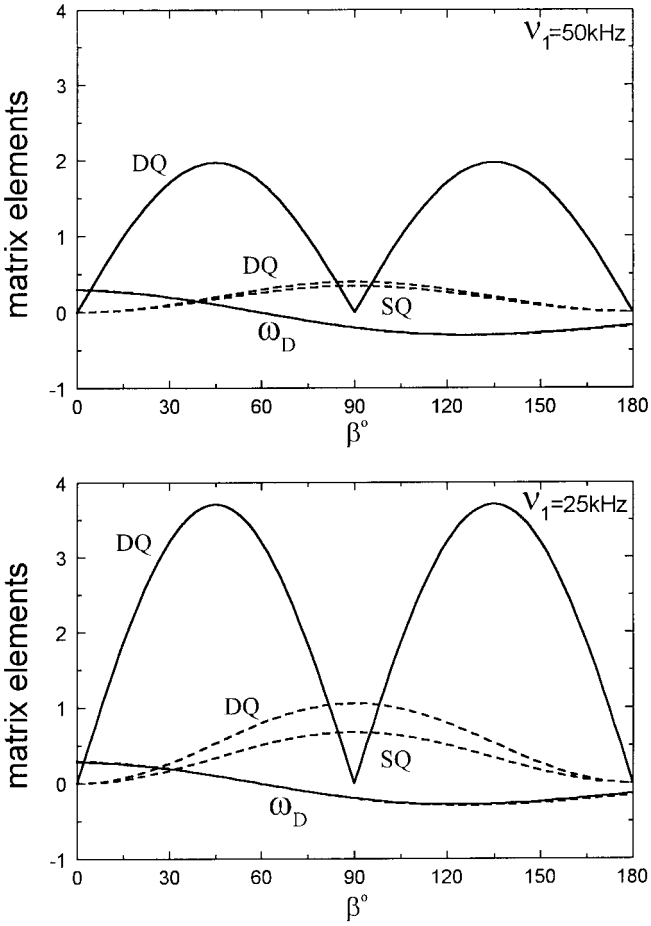

FIG. 4. Magnitudes of the various matrix elements of the average Hamiltonians in Eqs. [13] and [18] are plotted for different orientations of the quadrupolar principal direction (β is given wrt the rotor main direction). The effect of the CPL sequence on two different B_1 fields is shown for the dipolar vector oriented 60° from the quadrupolar principal direction. $\phi = 0°$, $\gamma = 10°$, $\alpha = 0°$.

with

$$(I_x^{12} - I_x^{23}) + (I_x^{45} - I_x^{56}) = \frac{1}{\sqrt{2}}(S_xS_z + S_zS_x), \qquad [19]$$

where the $I_y^{i,j}$ operators contribute to the imaginary part of the matrix elements of $I_x^{i,j}$. The coefficients of Eq. [18] are integrals of the same type as in Eq. [15].

To investigate the improvement of the REDOR dephasing due to the application of the CPL (composite pulse) sequences, we must thus examine the effect of the single-quantum (SQ) terms with ω_{xz}, ω_{yz} in Eq. [18] on the spin system. These terms appear in $H^{(0)}$ in addition to the terms of Eq. [13]. In Fig. 4 the magnitudes of the various matrix elements of the average Hamiltonians in Eqs. [13] and [18] are compared for some arbitrary crystallite orientation. This figure shows that the magnitudes of the coefficients of the double-quantum (DQ) off-diagonal terms are much smaller in the CPL case than in the case of *XY*-4. According to the expression for the REDOR signal in Eq. [16], this decrease will increase the overall REDOR decay of the powder by a reduction of the values of ϕ.

The SQ elements of magnitude $\sqrt{\tilde{\omega}_{xz}^2 + \tilde{\omega}_{yz}^2}$ in the CPL case cause oscillations of the I_x^{25} term of ρ_0. In the limit when the SQ terms are larger than the dipolar terms, they will again equalize the two Hamiltonians $H^{\alpha(0)}$ and $H^{\beta(0)}$ and no REDOR oscillation can be expected. Thus the SQ matrix elements will influence the I_x^{25} term only when they are of the same order of magnitude as the dipolar interaction element $\tilde{\omega}_D$. Then a cooperative mechanism, involving both the dipolar interaction and the quadrupolar interaction through the SQ elements, will result in a REDOR decay beyond $\frac{1}{3}$. This effect can be shown quantitatively for a single crystallite by a diagonalization of the matrix representations of $H^{\alpha(0)}$ and $H^{\beta(0)}$ of Eq. [18], and a transformation of I_x to their diagonal representation. The results of such a calculation are shown in Fig. 5. In this figure the zero-order time-independent part of the REDOR signal is plotted as a function of Euler angle β of the quadrupolar tensor in the rotor frame. As can be seen, the contribution of the SQ elements reduces this part of the signal (solid line) to values below $\frac{1}{3}$ for certain values of β. The exact shape of this line depends on the polar angle θ between the dipolar vector and the principal direction of the quadrupolar tensor ($\theta = 30°$ in our case). The dashed curve shows the same contribution when the SQ terms are neglected in the calculation. We see that the two curves overlap in the regions where the dipolar term is small (see $\tilde{\omega}_D$ in Fig. 4). We should emphasize here that for large

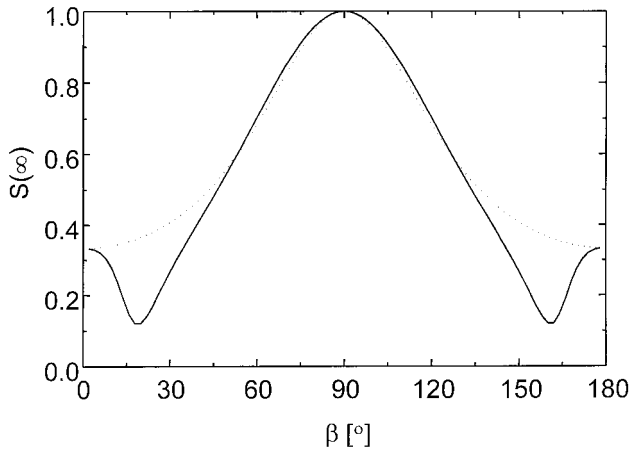

FIG. 5. The normalized zero-order time-independent part of the REDOR signal $S(\infty)$ is plotted as a function of the Euler angle β of the quadrupolar tensor in the rotor frame. The solid line shows the calculated $S(\infty)$ resulting from the zero-order average Hamiltonian in Eq. [18]. The dashed line represents the same, while omitting the SQ terms in the calculation. The values of the parameters used in the calculation were QCC = 146 kHz for the $I = 1$ spin, $\nu_d = 1.64$ kHz for the dipolar interaction constant between ^{2}H and ^{15}N, $\theta = 30°$ for the polar angle between principal direction of the quadrupolar tensor and the dipolar vector, $\nu_r = 4$ kHz for the spinning speed, and $B_1 = 38$ kHz for the RF field strength.

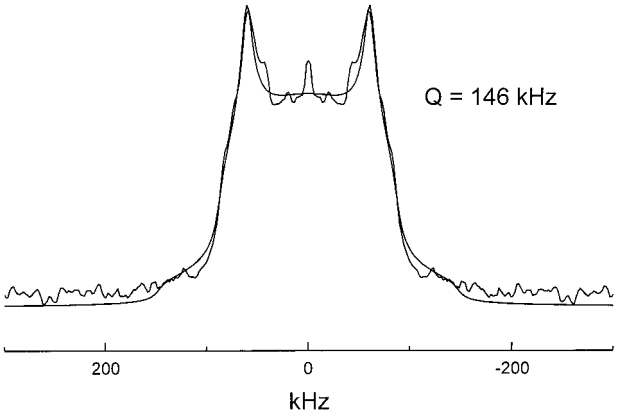

FIG. 6. Static ^{2}H spectrum of acetanilide recorded (experiment and simulation with $Q = 146$ kHz and $B_1(^2\text{H}) = 100$ kHz).

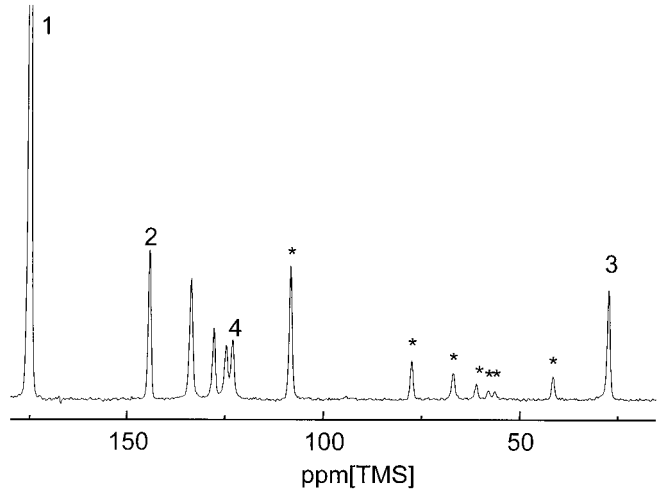

FIG. 7. ^{13}C CP-MAS spectrum and spectral assignment of acetanilide, measured under the same conditions as the REDOR spectra (the asterisks mark spinning sidebands).

dipolar interactions higher order effects become significant and the powder signals can decay toward zero. This can be shown by exact numerical simulations.

We can thus conclude that the CPL sequences indeed improve the powder REDOR decay rate and its overall decay, the first due to reduction of the DQ terms and the latter due to the appearance of SQ terms in the average toggling frame Hamiltonian.

RESULTS

X–^{2}H REDOR experiments have been performed on doubly ^{2}H–^{15}N-labeled acetanilide (**I**) ($X = {}^{15}$N) and on singly ^{2}H (**II**)-labeled and doubly ^{2}H–^{13}CO (**III**)-labeled acetanilide ($X = {}^{13}$C). The ^{15}N spectrum (not shown) of (**I**) consists of a single line, caused by the amide nitrogen. The ^{2}H quadrupolar echo spectrum (Fig. 6) exhibits a typical ^{2}H powder pattern with a quadrupolar splitting of 146 kHz. Figure 7 displays the natural abundant ^{13}C CP-MAS spectrum of (**II**), marking the lines where a REDOR effect was observed. The REDOR experiments on the directly bonded spin pair ^{2}H–^{15}N in (**I**) were performed mainly to compare the efficiency of the different pulse sequences. In the ^{2}H–^{13}C REDOR experiments on (**II**) the dephasing of the carbons, assigned in Fig. 7, was accomplished by the use of the 90_x–180_y–90_x composite pulse scheme.

^{2}H–^{15}N REDOR Results

Figure 8 compares the simulated and experimental and ^{15}N-detected S/S_0 REDOR results of (**I**) for the three pulse sequences presented in Fig. 2 with the theoretical REDOR decay curves under the influence of ideal 180° δ pulses. The symbols mark the experimental data and the solid lines the simulations of the decay curves. The dashed line corresponds to the δ-pulse result. All experiments and calculations have been performed with ^{15}N on resonance. In the simulations an axially symmetric quadrupolar tensor, with its symmetry axis parallel to the ND bond vector, was taken and the dephasing was evaluated for a dipolar coupling of 1.64 kHz. For the three pulse sequences a REDOR dephasing was found with an initial slope that is slower than the calculated dephasing caused by δ pulses on the deuterons by a factor of about 3–4. Another significant difference is that the S/S_0 values approach zero in all the experiments and calculations with real pulses but reach $\frac{1}{3}$ for the δ pulses. The fastest dephasing is obtained for the 90_x–180_y–90_x composite pulses, followed by results of the 90_x–90_y–90_x pulses. The dephasing of the simple 180_x pulses is significantly less efficient than the dephasing of the other two sequences. While the calculated REDOR decay curves of the composite pulse sequences reproduce the experimental data fairly closely, the simulated dephasing of the 180_x pulse gives an underestimated value for S/S_0 for large τ values. A possible

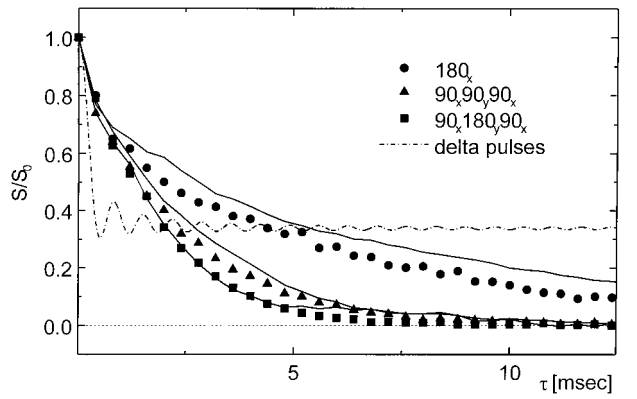

FIG. 8. REDOR results on ^{15}N–^{2}H doubly labeled acetanilide. The symbols mark the experimental data and the solid lines the simulations of the decay curves using $Q = 146$ kHz, $B_1(^2\text{H}) = 37$ kHz, $B_1(^{15}\text{N}) = 31$ kHz, and $D = 1.64$ kHz. The dashed line compares these decays to the decay corresponding to δ pulses (i.e., $B_1(^2\text{H}) \gg Q$).

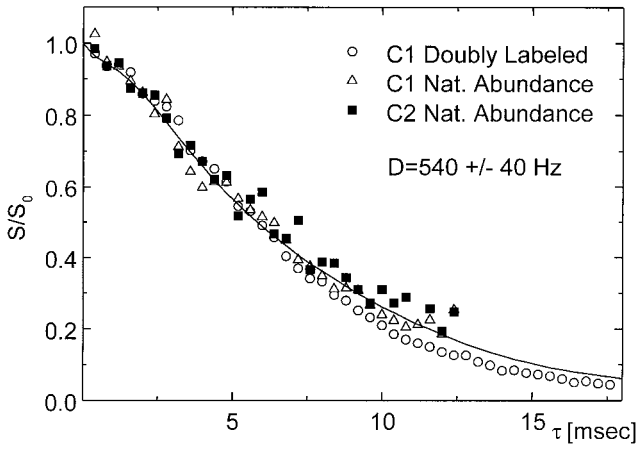

FIG. 9. ^{13}C natural abundance ^{2}H-labeled REDOR results of the acetanilide α-carbons C_1 and C_2. Both carbons exhibit the same dipolar coupling. The solid line shows the simulation of the data using D = 540 Hz, $B_1(^2\mathrm{H})$ = 33 kHz, $B_1(^{13}\mathrm{C})$ = 33 kHz, and Q = 146 kHz.

reason for the deviations at large τ values is an additional dephasing due to intermolecular couplings. We found in the calculations that the actual decay curves depend rather critically on the values of the quadrupolar frequency as well as on the B_1 field applied to the ^{2}H atoms.

^{2}H–^{13}C REDOR Results

The carbon-detected ^{2}H–^{13}C REDOR results can be divided into the α carbons C_1 and C_2, which are directly bonded to the amide nitrogen, and the β carbons C_3 and C_4, which are two bonds away from the nitrogen. Figure 9 presents the results of the ^{2}H–^{13}C REDOR experiments on the α carbons C_1 and C_2. The experiments were performed on a ^{13}C-labeled sample (**III**) at the α–CO position and on a nonlabeled sample (**II**). The 90_x–180_y–90_x composite pulse sequence on the deuterons was employed for these experiments. The solid line shows the result of a simulation of the REDOR decay curve using a dipolar coupling of 540 Hz. To cover most of the experimental points a spread of about 80 Hz is necessary. The dipolar interaction of 540 ± 40 Hz corresponds to a distance of 2.05 ± 0.05 Å.

Figure 10 presents the results from the natural abundance ^{13}C REDOR results of the β carbons C_3 and C_4 in (**II**). As a result of the less perfect suppression of off-resonance effects due to the simple *XY* phase cycling there are some small-amplitude oscillations in the dephasing visible in the decay curve of C_4 (Fig. 10), which do not cause any problems in the evaluation of the data, however. Despite the fluctuations in the experimental results due to the small REDOR dephasings, the C_4 carbons show a slightly faster decay than the C_3 carbons. This suggests a difference between the CD distances of these two carbon atoms. The solid lines mark the average results of the simulations that best fit the experimental results. These simulations correspond to a coupling of 270 ± 20 Hz for the C_3 carbons and of 300 ± 40 Hz for the C_4 carbons, corresponding to a nuclear distance of 2.58 ± 0.06 and 2.49 ± 0.12 Å, respectively.

DISCUSSION

The REDOR dephasing of a spin-$\frac{1}{2}$ nucleus coupled to a deuterium spin-1 nucleus is rather insufficient in the case of a large deuterium quadrupolar interaction and relatively weak 180 pulses applied to each rotor cycle on the deuterons. REDOR and REAPDOR methods, in which all except for one 180 pulse are applied in the spin-$\frac{1}{2}$ channel, could provide alternative approaches that increase the dipolar dephasing. In this publication we have reported the use of 90_x–180_y–90_x and 90_x–90_y–90_x composite pulses that replace standard 180 pulses on the deuterons. We have shown experimentally and theoretically that the application of these composite pulse sequences improves the REDOR dephasing significantly. For small and intermediate spinning frequencies (<10 kHz) and RF amplitudes down to 20 kHz the CPL sequences can be made much shorter than the rotor periods and can therefore be easily implemented into the rotor cycle. They can cause an increase of the overall REDOR decay rates of up to about two times the rates obtained with 180 pulses. Using the CPL sequences we have measured in acetanilide ^{13}C–^{2}H dipolar couplings in the range from 250 to 550 Hz, corresponding to ^{13}C and ^{2}H atom pairs that are separated by two or three covalent bonds. The quantitative analysis of the experimental data was performed by numerically solving the kinetic equation of the density matrix under the influence of the various interaction terms in the spin-Hamiltonian and finite RF pulse lengths. After careful calibration of all NMR parameters and measurement of the relevant NMR interaction tensors it was possible to directly evaluate the X–^{2}H REDOR results, without

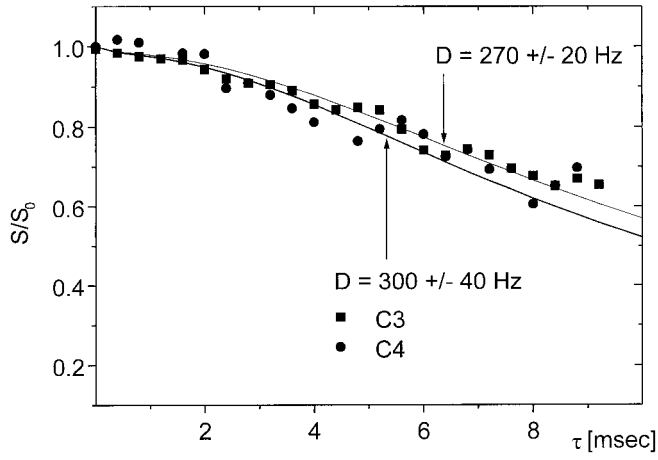

FIG. 10. ^{13}C natural abundance ^{2}H-labeled REDOR results of the acetanilide β carbons C_3 and C_4. The carbons exhibit different dipolar couplings. The solid lines show the simulation of the data using D = 0.27 kHz (C_3) and D = 0.30 kHz (C_4), $B_1(^2\mathrm{H})$ = 33 kHz, $B_1(^{13}\mathrm{C})$ = 33 kHz, and Q = 146 kHz.

TABLE 1
Summary of Experimental Data

	r/Å[a]	r/Å[b]	r/Å[c]	r/Å[d]	D/Hz[d]	D/Hz[e]	r/Å[e]
C_1	2.132	1.936	2.039	2.019	564	540 ± 40	2.05 ± 0.05
C_2	2.053	1.972	2.064	2.051	538	540 ± 40	2.05 ± 0.05
C_3	2.603	2.474	2.513	2.499	297	270 ± 20	2.58 ± 0.06
C_4	2.438	2.476	2.506	2.504	295	300 ± 40	2.49 ± 0.12
N	1.08	0.896	1.020	1.007	1810	1640 ± 40	1.04 ± 0.09
						1640 ± 40[f]	1.04 ± 0.09

[a] X-ray 295 K (*29*).
[b] X-ray 113 K (*28*).
[c] Neutron diffraction 15 K (*30*).
[d] Neutron diffraction 295 K (*30*).
[e] NMR ^{2}H REDOR.
[f] ^{15}N NMR lineshape analysis 295 K (*9, 10*).

the necessity of introducing any fit parameters or employing a calibration measurement.

Table 1 compiles the distances obtained from our REDOR experiments and compares them with distances obtained by diffraction techniques. There are some discrepancies between the diffraction data. While the new X-ray (*28*) and the neutron diffraction data (*30*) state that the C_1D distance (see Fig. 1) is shorter than the C_2D distance and the C_3D and C_4D distance are essentially the same, the older X-ray study (*29*) states the opposite, i.e., the C_1D distance is longer than the C_2D distance and the C_3 distance is longer than the C_4 distance. In addition, there are strong deviations between the reported NH distances. These differences can probably be attributed to the well-known difficulty of localizing hydrons with X-ray spectroscopy.

For a quantitative comparison to our REDOR data the neutron diffraction data at 295 K (*30*) and NMR lineshape results at room temperature are particularly important, since the position of the hydrogens depends on temperature, as is evident from the difference between distances obtained from neutron diffraction at 15 and 295 K. Comparing the high-temperature neutron diffraction data with our data shows good agreement. The observed difference between the C_1D (2.019 Å) and C_2D (2.051 Å) distances could not be resolved in our experiments (2.05 ± 0.05 Å). A slight discrepancy between our NMR results for the ND distance to the NH distance obtained from neutron diffraction is observed. Neutron scattering measures a NH distance of 1.007 Å (*30*) at $T = 295$ K, while our REDOR data give 1.04 ± 0.01 Å, corroborating previous results from NMR lineshape analyses (*9, 10*) on ^{15}N–^{2}H doubly labeled acetanilide.

There are two possible explanations for these differences between the NMR data and neutron diffraction data, which are not necessarily mutually exclusive:

(i) The hydron is part of the —NH$^{\cdots}$ O═C— hydrogen bond. It is well known that the positions of the hydron and the deuteron in these bonds are different due to ^{1}H/^{2}H isotope effects (*8*).

(ii) Fast vibrational motions of the molecule cause a partial averaging of the dipolar interaction, which results in a slight decrease of the distance measured by NMR spectroscopy (*5*).

Besides this small difference the structure of acetanilide found from REDOR is in good agreement with the structure determined by scattering methods.

It must be emphasized that the calculated REDOR decay curves depend strongly on the value of the deuterium B_1 field strengths in addition to its dependence on pulse settings, the dipolar interaction strengths, and quadrupolar couplings. They also depend, although to a lesser extent, on the relative orientation of the dipolar vector with respect to the quadrupolar tensor. For example, in the coupling regime of C_3 and C_4 (300 Hz), changes in the ^{2}H B_1 field or quadrupolar coupling of ±1 kHz lead to a difference in the determined dipolar coupling of ±5 Hz, i.e., ca. 2%. Since the observed REDOR curves are practically featureless there are various sets of parameters which are in principle capable of fitting the same decay curve. Therefore, a direct quantitative evaluation of the distances, using the CPL REDOR approach, is possible only if the experimental NMR parameters of the system are well known.

If this is not the case a second strategy can be employed. It is evident that the decay curves of different carbons coupled to the same ^{2}H nucleus or to ^{2}H nuclei in the same functional group are not independent of each other and should be analyzed with the same strength of quadrupolar interaction. Hence, it follows that the relative sizes of the couplings of spins to the same type of deuteron can be elucidated even if the absolute sizes of the couplings are difficult to determine. In most situations a calibration of these relative couplings to absolute values can be performed by using either a calibration experiment on a chemically similar reference compound, with deuterons in the same functional group, or a measurement of a well-known distance in the studied molecule, for example, a direct CD bond or a CND distance. In our system it would have been possible, instead of simulating all decay curves as described above, to use as an internal standard the known distance between the carbonyl carbon C1 and the deuteron.

CONCLUSION

It has been shown that, when composite pulses are employed on the deuterons, X–^{2}H REDOR is a powerful technique for studying molecular conformations of molecules, even for weak ^{2}H B_1 fields and strong ^{2}H quadrupolar interactions. The investigated 90_x–180_y–90_x and 90_x–90_y–90_x CPL have proven far superior to the simple 180 pulses, introducing an approximately two times faster dipolar dephasing, thus effectively enlarging the range of weak dipolar couplings measurable by X–^{2}H REDOR spectroscopy. Using a careful calibration of all NMR parameters it is feasible to analyze these experiments directly by numerical simulations. For quantitative applications of X–^{2}H REDOR on compounds, where not

all NMR parameters are known exactly, it is necessary to perform a reference experiment either on a standard compound or alternatively on a X–^{2}H pair with known distance in the measured compounds themselves. As an experimental example the molecular geometry of acetanilide has been studied by this method and compared to diffraction data. In conclusion it has been shown that X–^{2}H REDOR spectroscopy is well suited to the localization of hydrons in organic compounds.

EXPERIMENTAL

Sample

The synthesis of isotopically labeled acetanilide was performed by the standard procedures (*35*) of adding a solution of acetyl chloride (either unlabeled or 99% ^{13}C(CO)-labeled from Chemotrade, Leipzig, Germany) in chloroform to aniline (either unlabeled or 99% ^{15}N-labeled, also from Chemotrade) dissolved in chloroform and stirred in an ice bath. The addition was completed at a higher temperature of about 50°C. The solution was stirred for 1 h and the excess solvent removed to yield crystals of acetanilide which were recrystallized in water. These crystals were selectively deuterated in the exchanging amide position by dissolving twice in excess CH_3OD, waiting for 2 h at room temperature, and then drying under vacuum. After this procedure the deuterium labeling was better than 99%.

Due to the size of the acetanilide molecule, the expected intermolecular dipolar couplings are relatively weak. For example, the largest intermolecular ^{15}N–^{2}H coupling can be estimated as 37 Hz from the crystal structure, which has only a nonnegligible influence on the REDOR dephasing of the X nucleus for very long recoupling times. Therefore no isotope dilution of the samples was performed.

Spectrometer

A detailed discussion of our homebuilt three-channel NMR spectrometer has been given recently (*10*). Here only some salient features are given. All experiments were performed at a field of 6.98 T, corresponding to a proton resonance frequency of 297.8 MHz on a standard Oxford wide-bore magnet (89 mm) equipped with a room-temperature shim unit. For the proton channel a Creative Electronics 1-kW class C amplifier was used. For the ^{15}N or ^{13}C channel a 1-kW class AB and for the ^{2}H channel a 2-kW class AB amplifier, both from AMT, were employed. All amplifiers are equipped with RF blanking to suppress noise during data acquisition. The static ^{2}H spectrum of acetanilide was recorded with a homebuilt single-resonant ^{2}H NMR probe using the 90_x–90_y echo sequence with $B_1(^2\mathrm{H}) = 100$ kHz. All other experiments were performed using a Bruker triple-resonance NMR probe operating at room temperature. To improve the mutual RF isolation of the three channels commercial bandpass filters (Texscan) were employed in conjunction with homebuilt notch filters. The RF of the observed channel was fed through a crossed-diode duplexer connected to the detection preamplifier and through the filters into the probe. The other two channels were fed directly through the filters into the probe. The typical 90° pulse width was 6.5 μs for all three channels, corresponding to 38-kHz B_1 field in frequency units. For the proton decoupling the ^{1}H B_1 was changed to 52 kHz to avoid unwanted cross-polarization by mismatching the Hartmann–Hahn condition and to improve the decoupling efficiency. This was sufficient to remove ^{1}H–X dipolar line broadening. The repetition time of the experiments was 30 s for the acetanilide. All MAS spectra were recorded at a rotation frequency of 5 kHz, employing standard CYCLOPS phase cycling for data acquisition and XY phase cycling for the REDOR pulses. The rotation frequency was controlled using a Doty spin rate controller. Deviations in the rotation frequency were below 5 Hz. The spectra were measured by first cross-polarizing the observed nucleus from the protons and then recording the signal of the observed X nuclei under proton decoupling. The application of phase cycling schemes (*24*), like XY-8 or XY-16, in the dephasing channel, is not sufficient to compensate for the influence of the large quadrupolar broadening on the REDOR decays. We therefore used a composite pulse approach in the dephasing channel in conjunction with numerical simulation of the REDOR decay curves. The CPL were phase cycled in the XY scheme and put mirror symmetric with respect to the central echo scheme into the rotor periods. As an advantage of this simpler phase cycling scheme fewer cycle propagators have to be calculated in the numerical evaluation of the data. From these spectra the decay curves of the individual lines were determined and the REDOR decay curves were calculated by normalizing the decay employing the usual reference experiment without pulses in the dephasing channel.

APPENDIX A

Explicit Representation of the Functions $g_x(t)$, $g_y(t)$, and $g_z(t)$

An XY-4 REDOR pulse sequence that is applied on the ^{2}H spins during two rotor periods is shown schematically at the top of Table A1. The pulses with an intensity ω_p have a length $t_p = \pi/\omega_p$ and are applied at $t = 0$, $T_R/2$, T_R, $3/2T_R$. In the table the periodic g_p functions are defined for all time intervals ①–⑧. The coefficients $g_{pq} = g_p g_q$ are used in the calculations.

A composite pulse sequence that is applied on the ^{2}H spins during one rotor period is shown schematically at the top of Table A2. The pulses with an intensity ω_p have a length $t_p = \pi/(2\omega_p)$ and are applied at $t = 0$, $t_p/2$, t_p, $3/2t_p$, and $T_R/2$, $T_R/2 + T_R/2$, $T_R/2 + t_p$, $T_R/2 + 3/2t_p$. In the table the periodic g_p functions are defined for all time

TABLE A1
Explicit Representation of the Functions $g_x(t)$, $g_y(t)$, $g_z(t)$ for the *XY*-4 REDOR

①	②	③	④	⑤	⑥	⑦	⑧
t_{py}	$T_R/2 - t_p$	t_{px}	$T_R/2 - t_p$	t_{py}	$T_R/2 - t_p$	t_{px}	$T_R/2 - t_p$
0		$T_R/2$		T_R		$3T_R/2$	$2T_R$

XY-4 REDOR sequence

	g_z	g_x	g_y
①	$\cos(\omega_p/2*t)$	0	$-\sin(\omega_p/2*t)$
②	-1	0	0
③	$-\cos(\omega_p/2*(t - T_R/2))$	$-\sin(\omega_p/2*(t - T_R/2))$	0
④	1	0	0
⑤	$\cos(\omega_p/2*(t - T_R))$	0	$\sin(\omega_p/2*(t - T_R))$
⑥	-1	0	0
⑦	$-\cos(\omega_p/2*(t - 3T_R/2))$	$\sin(\omega_p/2*(t - 3T_R/2))$	0
⑧	1	0	0

intervals ①–⑧. The coefficients $g_{pq} = g_p g_q$ are used in the calculations.

APPENDIX B

Derivation of Eq. [16]

In this appendix we present a short derivation of the expression for the signal in Eq. [16]. The signal is equal to

$$S(t) = \mathrm{Tr}(S_x(t)S^-), \qquad [A1]$$

where the time dependence of the initial density matrix S_x is determined by the average Hamiltonian, defined in Eq. [13]. This Hamiltonian can be represented in matrix form in the basis set defined in Eq. [7]. This 6×6 matrix $\boldsymbol{H}$ can be divided into two 3×3 matrices,

$$H^{\alpha(0)} = \frac{1}{2}\begin{pmatrix} \tilde{\omega}_D + \tilde{\omega}_{zz} & 0 & \tilde{\omega}_{xx} \\ 0 & -2\tilde{\omega}_{zz} & 0 \\ \tilde{\omega}_{xx} & 0 & -\tilde{\omega}_D + \tilde{\omega}_{zz} \end{pmatrix}$$

$$H^{\beta(0)} = \frac{1}{2}\begin{pmatrix} -\tilde{\omega}_D + \tilde{\omega}_{zz} & 0 & \tilde{\omega}_{xx} \\ 0 & -2\tilde{\omega}_{zz} & 0 \\ \tilde{\omega}_{xx} & 0 & \tilde{\omega}_D + \tilde{\omega}_{zz} \end{pmatrix} \qquad [A2]$$

with

$$H^{(0)} = \begin{pmatrix} H^{\alpha(0)} & 0 \\ 0 & H^{\alpha(0)} \end{pmatrix} \qquad [A3]$$

and can be diagonalized by a matrix Δ,

$$\Delta = \begin{pmatrix} \boldsymbol{D} & 0 \\ 0 & \boldsymbol{D}^{-1} \end{pmatrix} \qquad [A4]$$

with $\Lambda = \Delta \boldsymbol{H} \Delta^{-1}$,

$$\Lambda^{\alpha(0)} = DH^{\alpha(0)}D^{-1} = \frac{1}{2}\begin{pmatrix} \tilde{\omega}_D^{\mathrm{eff}} + \tilde{\omega}_{zz} & 0 & 0 \\ 0 & -2\tilde{\omega}_{zz} & 0 \\ 0 & 0 & -\tilde{\omega}_D^{\mathrm{eff}} + \tilde{\omega}_{zz} \end{pmatrix}$$

$$\Lambda^{\beta(0)} = D^{-1}H^{\beta(0)}D = \frac{1}{2}\begin{pmatrix} -\tilde{\omega}_D^{\mathrm{eff}} + \tilde{\omega}_{zz} & 0 & 0 \\ 0 & -2\tilde{\omega}_{zz} & 0 \\ 0 & 0 & \tilde{\omega}_D^{\mathrm{eff}} + \tilde{\omega}_{zz} \end{pmatrix} \qquad [A5]$$

TABLE A2
Explicit Representation of the Functions $g_x(t)$, $g_y(t)$, $g_z(t)$ for the CPL REDOR

①	②	③	④	⑤	⑥	⑦	⑧
$t_p/2_y$	$t_p/2_x$	$t_p/2_y$	$T_R/2 - 3t_p/3$	$t_p/2_y$	$t_p/2_x$	$t_p/2_y$	$T_R/2 - 3t_p/3$
0				$T_R/2$			T_R

Composite pulses

	g_z	g_x	g_y
①	$\cos(\omega_p/2*t)$	0	$-\sin(\omega_p/2*t)$
②	0	$\sin(\omega_p/2*(t - t_p/2))$	$-\cos(\omega_p/2*(t - t_p/2)$
③	$-\sin(\omega_p/2*(t - t_p))$	$\cos(\omega_p/2*(t - t_p))$	0
④	-1	0	0
⑤	$-\cos(\omega_p/2*(t - T_R/2))$	0	$\sin(\omega_p/2*(t - T_R/2))$
⑥	0	$-\sin(\omega_p/2*(t - T_R/2 - t_p/2))$	$\cos(\omega_p/2*(t - T_R/2 - t_p/2))$
⑦	$\sin(\omega_p/2*(t - T_R/2 - t_p))$	$-\cos(\omega_p/2*(t - T_R/2 - t_p))$	0
⑧	1	0	0

$$\boldsymbol{D} = \begin{pmatrix} \cos\phi/2 & 0 & -\sin\phi/2 \\ 0 & 1 & 0 \\ \sin\phi/2 & 0 & \cos\phi/2 \end{pmatrix} \qquad [A6]$$

and

$$\tilde{\omega}_{\mathrm{D}}^{\mathrm{eff}} = ((\tilde{\omega}_{\mathrm{D}})^2 + (\tilde{\omega}_{xx})^2)^{1/2}; \quad \tan\phi = \frac{\tilde{\omega}_{xx}}{\tilde{\omega}_D}. \qquad [A7]$$

The matrix representation of the operator $\boldsymbol{S}_x$ has the form

$$S_x = \frac{1}{2}\begin{pmatrix} 0 & I_d \\ I_d & 0 \end{pmatrix} \qquad [A8]$$

with $\boldsymbol{I}_d$ a 3×3 unit matrix.

The signal in Eq. [A1] can be evaluated by insertion of Eqs. [A4–A7] and $t = 2nT_{\mathrm{R}}$:

$$\begin{aligned} S(t) &= \mathrm{Tr}(\Delta \mathrm{e}^{-\mathrm{i}\Lambda t}\Delta^{-1} S_x \Delta \mathrm{e}^{\mathrm{i}\Lambda t}\Delta^{-1} S^-) \\ &= \mathrm{Tr}(\mathrm{e}^{-\mathrm{i}\Lambda^{\beta(0)}t} D^{-2} \mathrm{e}^{i\Lambda^{\alpha(0)}t} D^2), \end{aligned} \qquad [A9]$$

which has the explicit form of Eq. [16]:

$$S(t) = \tfrac{1}{3} + \tfrac{2}{3}(\cos^2\phi \cos\tilde{\omega}_{\mathrm{D}}^{\mathrm{eff}} t + \sin^2\phi). \qquad [A10]$$

ACKNOWLEDGMENTS

Support by the German Israel Foundation under G.I.F. Research Grant I-297.092.05/93 and by the Sonderforschungsbereich 448 "Mesoskopisch Strukturierte Verbundsysteme" of the Deutsche Forschungsgemeinschaft, as well as the Fonds der Chemischen Industrie, Frankfurt, is gratefully acknowledged.

REFERENCES

1. M. Mehring, "High Resolution NMR Spectroscopy in Solids," Springer-Verlag, Berlin/Heidelberg/New York (1983).
2. C. P. Slichter, "Principles of Magnetic Resonance," Third ed., Springer-Verlag, Berlin/Heidelberg/New York (1990).
3. R. Ernst, G. Bodenhausen, and A. Wokaun, "Principles of NMR in One and Two Dimensions," Clarendon, Oxford (1987).
4. K. Schmidt-Rohr and H. W. Spiess, "Multidimensional Solid State NMR and Polymers," Academic Press, London (1994).
5. C. G. Hoelger and H. H. Limbach, *J. Phys. Chem.* **98,** 11803 (1994).
6. C. G. Hoelger, F. Aguilar-Parilla, J. Elguero, O. Weintraub, S. Vega, and H. H. Limbach, *J. Magn. Res. A* **120,** 46 (1996).
7. H. Benedict, C. Hoelger, F. Aguilar-Parrilla, W. P. Fehlhammer, M. Wehlan, R. Janoschek, and H. H. Limbach, *J. Mol. Struct.* **378,** 11 (1996).
8. H. Benedict, H. H. Limbach, M. Wehlan, W. P. Fehlhammer, N. S. Golubev, and R. Janoschek, *J. Am. Chem. Soc.* **120,** 2939 (1998).
9. M. D. Lumsden, R. E. Wasylishen, K. Eichele, M. Schindler, G. H. Penner, W. P. Power, and R. D. Curtis, *J. Am. Chem. Soc.* **116,** 1403 (1994).
10. G. Buntkowsky, I. Sack, H.-H. Limbach, B. Kling, and J. Fuhrhop, *J. Phys. Chem. B* **101,** 11265 (1997).
11. M. Emshwiller, E. L. Hahn, and D. E. Kaplan, *Phys. Rev. Lett.* **118,** 414 (1960).
12. M. E. Stoll, A. J. Vega, and R. W. Vaughan, *J. Chem. Phys.* **65,** 4093 (1976).
13. J. S. Waugh, *Proc. Natl. Acad. Sci. USA* **73,** 1394 (1976).
14. T. Gullion and J. Schaefer, *Adv. Magn. Opt. Reson.* **13,** 57 (1989).
15. T. Gullion and J. Schaefer, *J. Magn. Reson.* **81,** 196 (1989).
16. J. Schaefer, E. O. Stejskal, and R. Buchdahl, *Macromolecules* **8,** 291 (1975).
17. T. Gullion, *Chem. Phys. Lett* **246,** 325 (1995).
18. L. Chopin, T. Gullion, and S. Vega, *J. Am. Chem. Soc.* **120,** 4406 (1998).
19. A. Schmidt, R. A. McKay, and J. Schaefer, *J. Magn. Res.* **96,** 644 (1992).
20. A. Schmidt, T. Kowalewski, and J. Schaefer, *Macromolecules* **26,** 1729 (1993).
21. C. A. Klug, P. Lani Lee, I. S. H. Lee, M. M. Kreevoy, R. Yaris, and J. Schaefer, *J. Phys. Chem. B* **101,** 8086 (1997).
22. P. L. Lee and J. Schaefer, *Macromolecules* **28,** 2577 (1995).
23. P. L. Lee and J. Schaefer, *Macromolecules* **28,** 1921 (1995).
24. T. Gullion, and J. Schaefer, *J. Magn. Reson.* **92,** 439 (1991).
25. Counsell, M. H. Levitt, and R. R. Ernst, *J. Magn. Reson.* **63,** 133 (1985).
26. M. H. Levitt, D. Suter, and R. R. Ernst, *J. Chem. Phys.* **80,** 3064 (1984).
27. M. H. Levitt, *Prog. NMR Spectrosc.* **18,** 61 (1986).
28. H. J. Wasserman, R. R. Ryan, and S. P. Layne, *Acta Crystallogr.* **41,** 783 (1985).
29. C. J. Brown, *Acta Crystallogr.* **21,** 442 (1966).
30. S. W. Johnson, J. Eckert, M. Barthes, R. K. McMullan, and M. Muller, *J. Phys. Chem.* **99,** 16253 (1995).
31. V. B. Cheng, H. H. Suzukawa, and M. Wolfsberg, *J. Chem. Phys.* **59,** 3992 (1973).
32. U. Haeberlen, "High Resolution NMR in Solids. Selective Averaging," Academic Press, New York (1976).
33. O. Weintraub and S. Vega, *J. Magn. Reson. A* **105,** 245 (1993).
34. A. E. Bennett, R. G. Griffin, and S. Vega, *Springer Ser. NMR* **33,** 1 (1994).
35. Organikum, VEB Verlag der Wissenschaften, Berlin (1986).